CONF-780769--1

LA-UR-78-2631

MASTER

TITLE: SEARCH FOR $\mu^+ \to e^+ \gamma$

AUTHOR(S): Martin D. Cooper

SUBMITTED TO: Proceedings of the 1978 Topical Conference on Weak Interactions

los alamos
scientific laboratory
of the University of California
LOS ALAMOS, NEW MEXICO 87545

An Affirmative Action/Equal Opportunity Employer

Form No. 836
St. No. 2629
1/75

UNITED STATES
ENERGY RESEARCH AND
DEVELOPMENT ADMINISTRATION
CONTRACT W-7405-ENG. 36

SEARCH FOR $\mu^+ \to e^+ \gamma$

Martin D. Cooper

Los Alamos Scientific Laboratory

University of California, Los Alamos, New Mexico 87545

Abstract

Using the Stopped Muon Channel at LAMPF to produce a surface muon beam, 2.3×10^{12} muons were stopped in a 50 mg/cm^2 target. The solid angle-efficiency product of the detector for the rare decay $\mu^+ \to e^+ \gamma$ was 1.2%. Hence, 3×10^{10} μ^+ decays were examined. There is no indication of any signal, the data being consistent with a small background of random electron and gamma coincidences. The new upper limit on the branching ratio is $\Gamma(\mu^+ \to e^+ \gamma)/\Gamma(\mu^+ \to e^+ \nu_e \bar{\nu}_\mu) < 2 \times 10^{-10}$ with 90% confidence.

The development of guage theories of weak and electromagnetic interactions has renewed interest in searching for the flavor violating decays of the muon. In particular, new searches for $\mu^+ \to e^+ \gamma$[1,2] and $\mu^- Z \to e^\pm Z'$[3] have taken place in the last two years. The theories predict that if all the masses of the neutrinos are not zero, then the flavors will not necessarily be eigenstates of mass and the physical particles will have admixtures of several flavors. Through these admixtures, muon number conservation will be violated. The upper limit one obtains from using the known limits on the mass of the muon and electron neutrinos is $\sim 10^{-24}$ and is experimentally uninteresting.

The discovery[4] of the τ tells us that the spectrum of lepton flavors is richer than previously believed. Various theories involving

heavy neutral leptons predict branching ratios as high as 10^{-8} for the muon number violating decays. The "standard" model uses the upper limit on the neutral τ mass of less than 250 MeV to predict branching ratios of less than 10^{-11}. This level of sensitivity has not yet been experimentally reached.

Other possibilities are still not experimentally ruled out. For example, the right handed electron and muon could be coupled to heavy right handed neutrinos as suggested by Cheng and Li.[5] Mixing of these heavy neutral leptons would possibly produce muon number violation at higher levels. Additionally, having more than one set of Higgs doublets which are mixed[6] would do the same. Other possibilities exist to produce muon number violation.

These theories all involve unknown particles with unknown mixing between particles. Hence, muon number violation may be at a level which is experimentally unobservable, or nature may have made it an exact symmetry for reasons we do not understand. Thus, if it is found, it is a useful testing ground for guage theories; if not, it only puts a weak limit on theories. The present published upper limits on muon number violation are given in Table 1.

The experiment described here was performed at the Clinton P. Anderson Meson Physics Facility (LAMPF) by a collaboration of scientists from Los Alamos, the University of Chicago, and Stanford University. They are listed in Table 2.

To search for the decay $\mu^+ \rightarrow e^+\gamma$ with a sensitivity of 10^{-10}, one must rely on kinematic separation from more favored processes. Normal muon decay produces a positron spectrum, the Michel Spectrum, which is peaked near half the muon mass, 1/2 x 105.6 MeV. In itself, it cannot be

Table 1. Present published upper limit on muon number violating decays.

Decay	Upper Limit (90% Confidence)	Reference
$\mu^+ \to e^+ \gamma$	2×10^{-10}	This work
	1.1×10^{-9}	2
$\mu^- + Z \to e^- + Z$ (Sulfer)	4×10^{-10}	3
$\mu^- + Z \to e^+ + (Z-2)$ (Sulfer)	1×10^{-9}	3
$\mu^+ \to e^+ \gamma\gamma$	5×10^{-8}	7
$\mu^+ \to e^+ e^+ e^-$	1.9×10^{-9}	8

Table 2. Participants in present work.

Name	Institutions
H. L. Anderson	University of Chicago, Los Alamos
J. D. Bowman	Los Alamos
R. Carrington	Stanford University
M. D. Cooper	Los Alamos
R. Eichler	Stanford University
M. E. Hamm	Los Alamos
C. M. Hoffman	Los Alamos
R. Hofstadter	Stanford University
E. B. Hughes	Stanford University
W. W. Kinnison	University of Chicago
H. S. Matis	University of Chicago, Los Alamos
T. McPharlane	Stanford University
R. E. Mischke	Los Alamos
D. E. Nagle	Los Alamos
J. S. Sarracino	Los Alamos
P. A. Thompson	Los Alamos
S. C. Wright	University of Chicago

mistaken for $\mu^+ \to e^+\gamma$ because it does not decay with a photon emission. However, it provides the high electron rate which can be in random coincidence with "photons" to simulate $\mu^+ \to e^+\gamma$. A prompt background comes from the radiative decay or internal bremsstrahlung in which a μ^+ decays into $e^+\gamma\bar{\nu}\nu$. Being a bremsstrahlung process, the angular correlation between the photon and positron is peaked near zero degrees and vanishes as one approaches the $\mu^+ \to e^+\gamma$ kinematics of positron and photon energy equal to 52.8 MeV and $\theta_{e\gamma} = 180^o$.

The experimental "tools" which have been used to distinguish between signal and background are a gamma ray resolution of 7.5%, a positron energy resolution of 8.3%, a timing resolution of 2.5 nsec, and an angular resolution of 5^o. Using these resolutions, we can demonstrate that the process $\pi^+ + Z \to (Z+1) + \pi^o \to e^+e^-\gamma$ is rejected at a level of 10^{-17}. The radiative decay is rejected at a level of 10^{-12}. Random backgrounds are only rejected at about a level of 10^{-10} and provide the major background for the experiment.

To discriminate against random coincidences, one must reduce the source of "photons" to a minimum. Cosmic rays and accelerator neutrons doing (n,p) reactions in the photon detector have been eliminated with shielding. The use of the surface muon beam, to be described below, eliminates positron annihilation-in-flight and external bremsstrahlung of positrons interacting in the target. Photons from radiative decay are always there and must be defeated with good energy resolution.

A critical part of the experiment was the surface muon beam. This beam of 30 MeV/c muons was derived from stopped pion decay in the last 50 mg/cm^2 of the proton production target. The 800 MeV beam of LAMPF was passed through a 6 gm/cm^2 C target. The low energy muons were

transported through a magnetic channel where pions decayed away. The beam was momentum analyzed and, then, purified by using the differential energy loss of positrons and muons in a 40 mg/cm^2 CH_2 degrader. Such a beam had the following advantages for a $\mu^+ \to e^+\gamma$ experiment: 1) Positron and pion contaminations of 10% and $<10^{-4}$ respectively, 2) Contaminent positron momentum substantially less than 52.8 MeV, 3) A rate of 2.5×10^6 Hz, and 4) A residual range of 30 mg/cm^2. The ability to use a 50 mg/cm^2 target eliminated the backgrounds from external bremsstrahlung and positron annihilation-in-flight as well as preserved the collinearity of e^+ and γ from $\mu^+ \to e^+\gamma$ which might otherwise be lost due to multiple scattering in the target.

The experimental apparatus for detecting $\mu^+ \to e^+\gamma$ is shown in Fig. 1. The beam enters the target through an iron shield to prevent deflection by the magnetic fields of the spectrometers. The target is supported by a cone shaped piece of 50 mg/cm^2 polyethylene shielding. This shielding catches any stray muons so that their decay positrons cannot pass through a thick piece of matter on the way toward the photon detector. Both arms of the detector are filled with He.

The positron arm consists of a magnetic spectrometer which bends 52.8 MeV/c particles by 40°. The incident and exiting angles are measured in four sets (x and y coordinates) of multiwire proportional counters (MWPC). Behind the MWPC's is a hodoscope of scintillation counters which are used both for timing and the trigger.

The photon arm consists of a photon detector and a sweeping magnet which prevents charged particles from hitting the photon counter. The photon detector is a multi-cellular array of NaI(Tl) made up of 45 hexagonal elements. A front view of these is shown in Fig. 2. Each

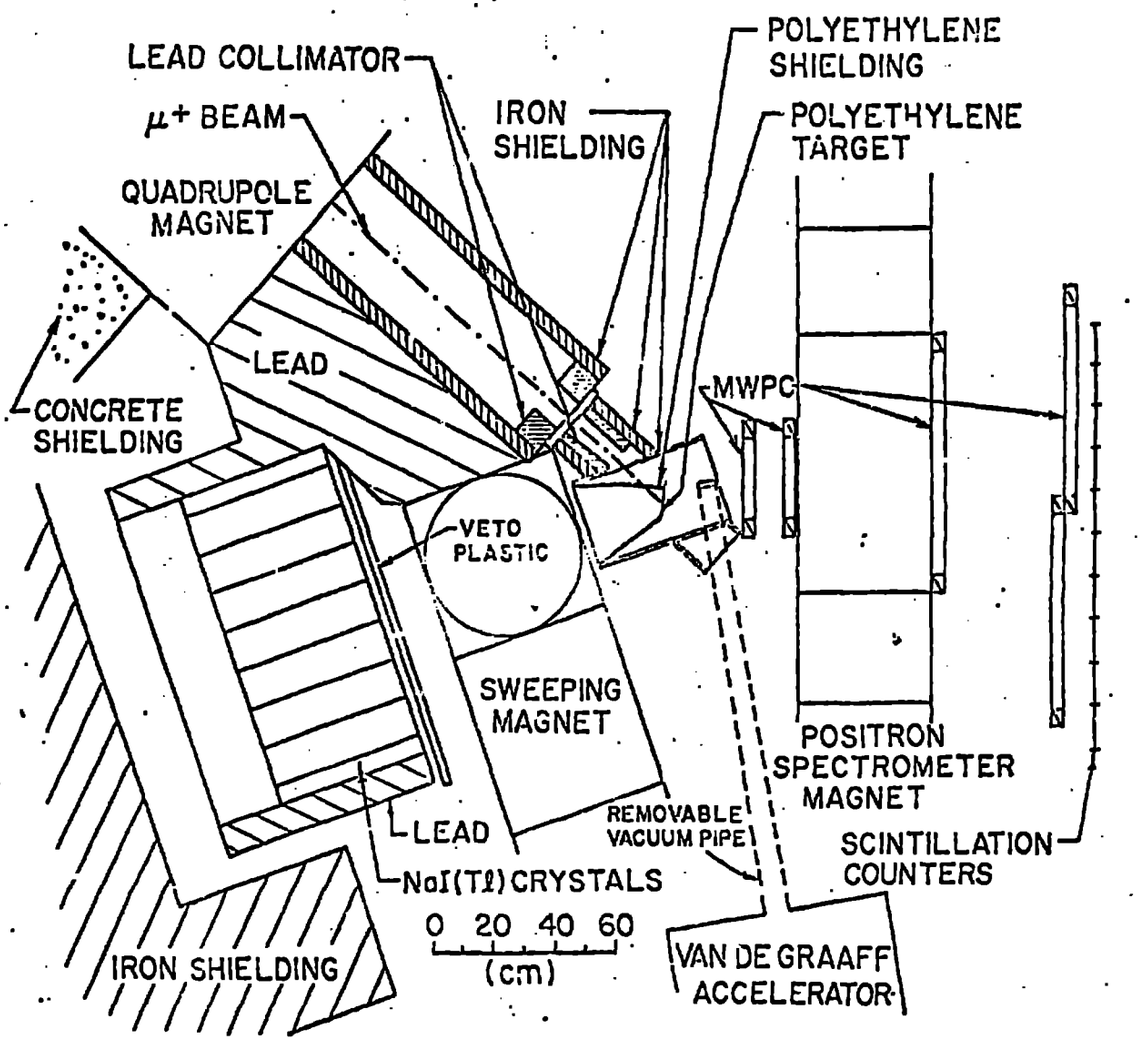

Figure 1. The experimental apparatus.

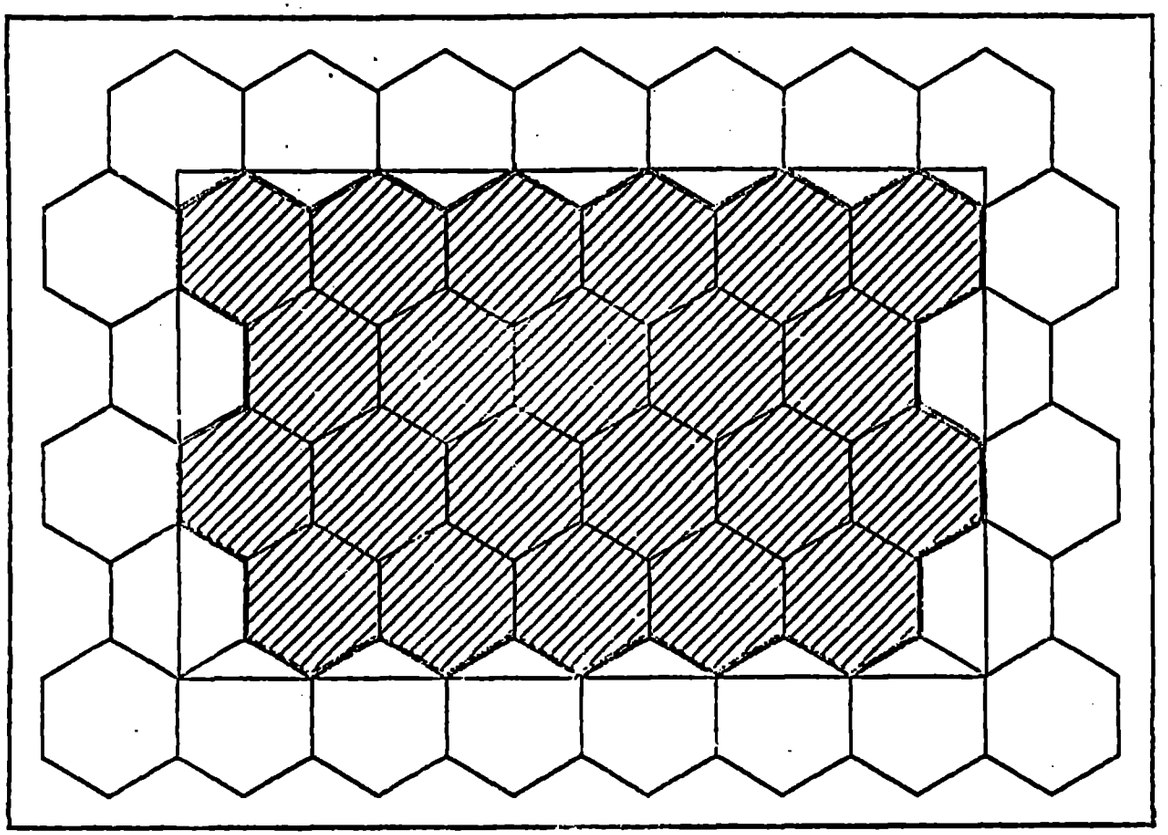

Figure 2. The front face of the NaI detector. The shaded region is the fiducial area and the inner rectangle represents the boundary of region shadowed by the field clamp.

crystal is 7.68 cm on a side and 20 radiation lengths deep. The edge crystals are shadowed by the sweeping magnet and its field clamp. They serve to contain showers which impinge on the fiducial crystals, which are cross hatched in the figure. The sweeping magnet keeps the singles rate in each crystal quite modest. The stack is also fronted by a charged particle veto counter.

The data from a typical trigger consists of timing information from the NaI and positron scintillators, sparks from the MWPC's, and pulse height information from the NaI array. The identification of $\mu^+ \to e^+\gamma$ candidates is dependent on finding time coincidence between the arms and a positron and photon, each of which has an energy $\gtrsim$ 30 MeV. The positron track is then reconstructed to give its initial positron and momentum at the target. The spread of the electromagnetic shower in the NaI is used to give an interaction point for the photon in the NaI. Assuming the same origin for both the photon and positron, the acollinearity angle is calculated.

With this description of how the apparatus is designed to work, it is now possible to understand the details of the experiment. The elements of a good $\mu^+ \to e^+\gamma$ experiment are examining enough μ decays and having enough background suppression to observe an effect at the level of the number of observed μ decays. In this experiment, both of these limitations occur around a level of 10^{-10}.

The number of μ decays in the experiment were measured in two ways. The first was to calculate the number of single positrons observed in the spectrometer. For an experiment dominated by random coincidences, the number of μ decays observed is just

$$N_\mu = N_\mu \text{ (observed in } e^+ \text{ arm)} \frac{fG}{R_\gamma \tau} \quad (1)$$

where f corrects N_μ (observed) for the energy acceptance of the spectrometer, G is the solid angle overlap of the arms, R_γ is the rate of γ singles, and τ is the resolving time of the trigger. The second measurement was taken from the number of decays into a calibrated counter times the acceptance of the spectrometer, which is calculated by Monte Carlo techniques. The two techniques agree to better than 10%. For the sample of data reported in this talk, the number of μ stops was 2.3×10^{12} and the number of μ decays which were examined was 3×10^{10}. This latter number is the denominator of the branching ratio calculation.

In order to know the level of background suppression, it is necessary to calibrate the detector and measure the resolution functions. The four quantities for which this must be done are the relative time between the arms t, the positron energy E_e, the γ-ray energy E_γ, and the acollinearity angle $\theta_{e\gamma}$.

To accomplish these measurements, an auxilliary calibration experiment was performed. The channel was reset to stop π^- in a liquid hydrogen target, where the reaction $\pi^- p \to \pi^0 n$ produced two high energy γ-rays from π^0 decay. One γ-ray was converted by pair production to a positron for observation in the positron spectrometer. The kinematics of the π^0 decay is dominated by Doppler shift from the π^0 motion. Here $\theta_{e\gamma}$ is restricted to be greater than 157°. For 180° decays, the two γ-rays have an energy of 55 and 82 MeV. The auxiliary experiment helps with the measurement of t, E_γ, and $\theta_{e\gamma}$.

The timing calibration was made with the π^0 decays. Relative offsets for each of the 45 NaI crystals and 10 hodoscopes were found so

that the coincidence peak lay at the zero of time. The timing resolution obtained from hydrogen was 2.2 nsec(FWHM). By relaxing the conditions on collinearity, a coincidence peak was observable in the data due to internal bremsstrahlung. The resolution of the peak was 2.5 nsec(FWHM) and is shown in Fig. 3. This resolution represents the coincidence requirement for the rejection of randoms since it is observed during the actual data taking.

The calibration of the electron spectrometer was accomplished by an optical survey of the position of the MWPC's, a map of the magnetic field along the entirety of the positron's path, and an analysis of field off data to demonstrate that, within the limits of multiple scattering, the positrons traced out straight lines. Then, regular data was analyzed to measure the Michel spectrum, shown in Fig. 4. Folding a bremsstrahlung corrected Michel spectrum with a Gaussian, a resolution of 8.3% (FWHM) and an offset of 0.3 MeV was obtained.

The energies and position algorithms for the NaI detector rely on the information from the crystal with the highest pulse height and its six adjacent neighbors as shown in Fig. 5. The choice of which crystals to include is a compromise between obtaining good resolution and preventing pile up. The energy algorithm consists of determining the energy deposited in each crystal as a function of the pulse amplitude. These functions are ideally linear, but may contain nonlinearities due to the phototubes and analog-to-digital converters. Once the crystal with the maximum energy is determined, events outside the feducial region are rejected. For the remaining events, the energy is the sum over the seven crystals.

Since the modular nature of the detector implies that the energy is divided over a large dynamic range, an elaborate calibration was

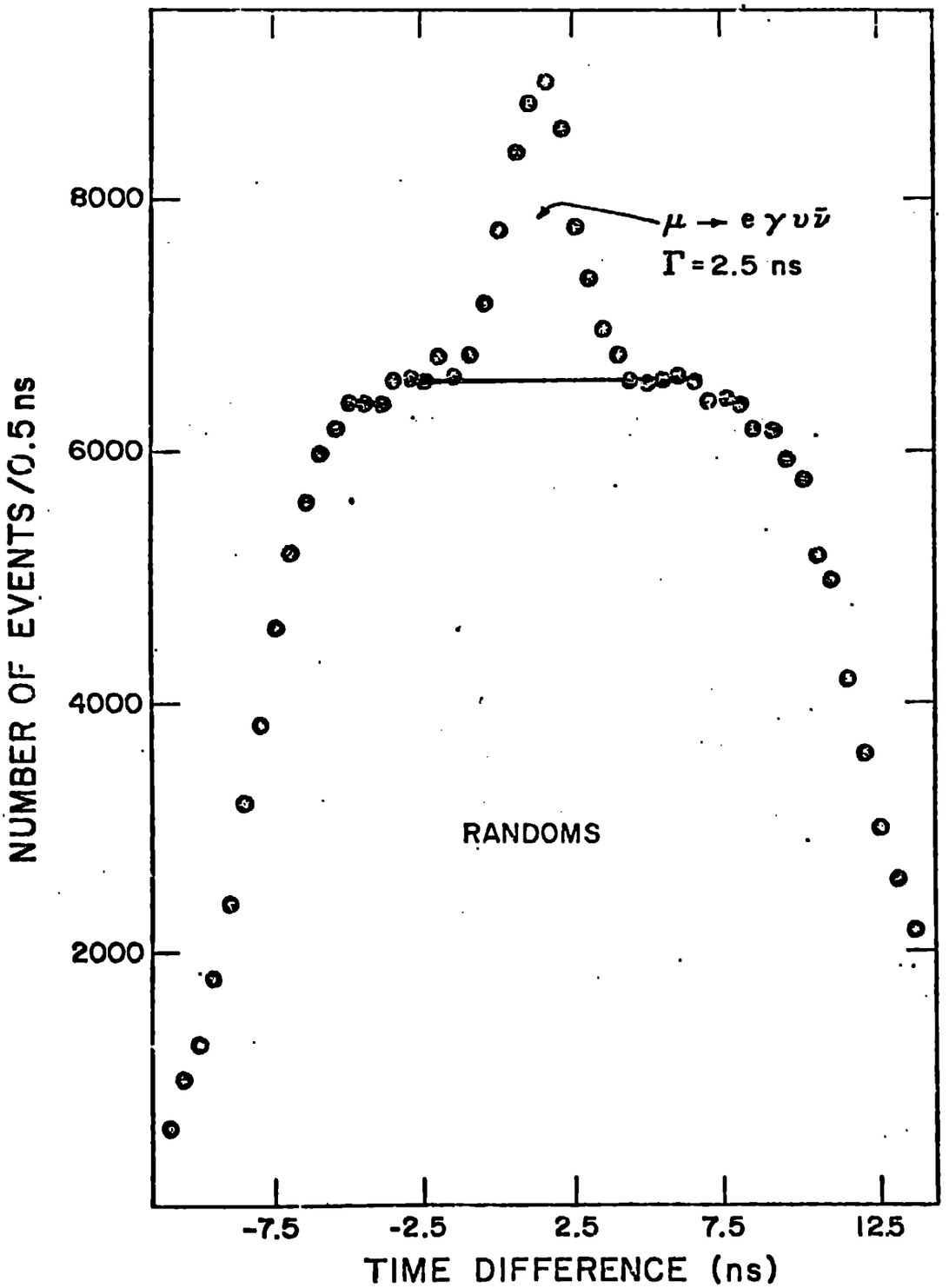

Figure 3. On line time spectrum with relaxed cuts on collinearity.

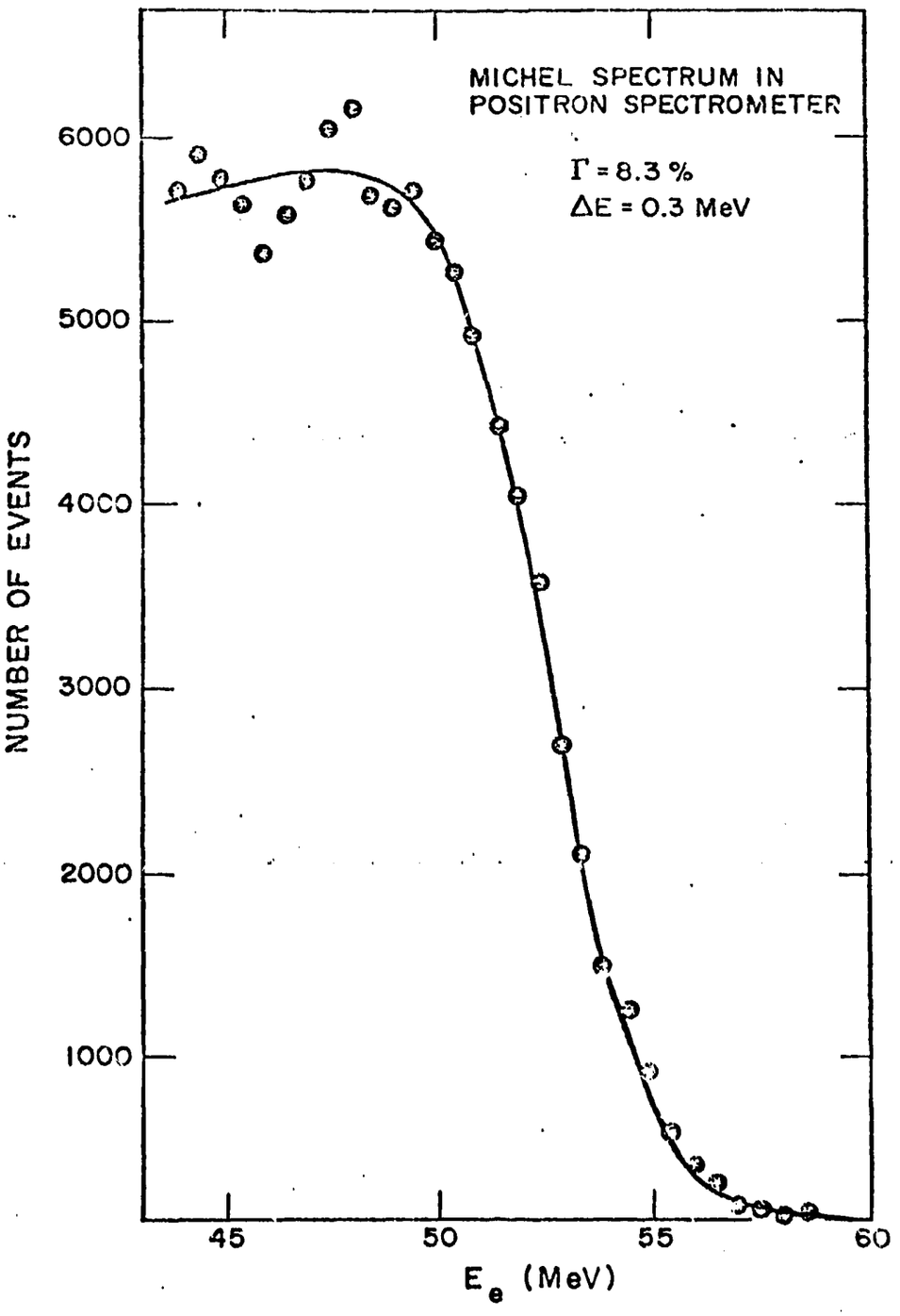

Figure 4. Michel spectrum in positron spectrometer.

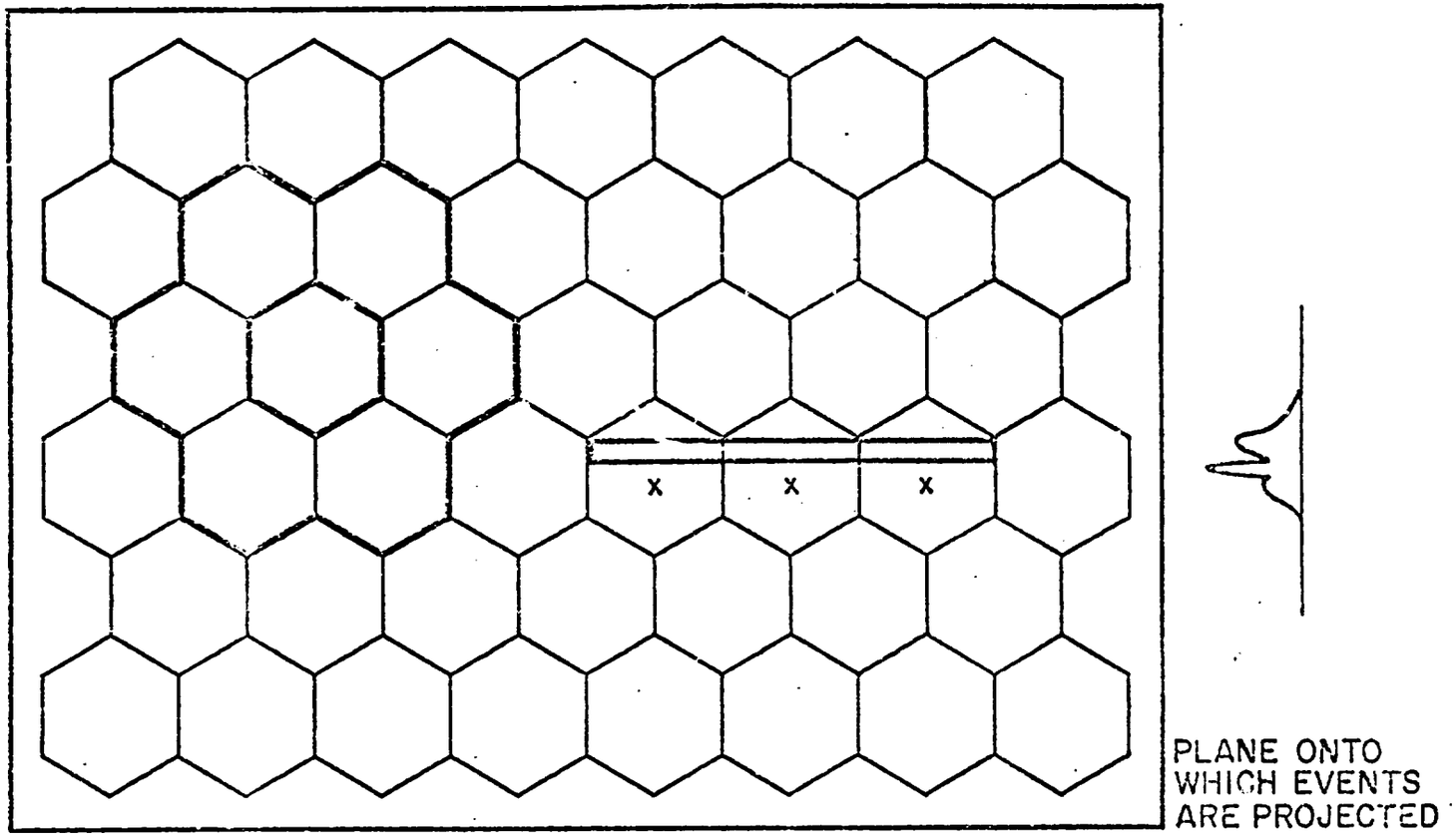

Figure 5. The front face of the NaI detector. Outlined in heavy ink is a typical sum of seven crystals used in the energy and position algorithms. The slot shows the location of the polyethylene slot in a Pb wall used to test the position algorithm. On the right is a sketch of the projection of the position data.

done with sufficient frequency to prevent drifts. In Table 3, each of the calibration points are listed, along with their fitted energy, resolution and frequency. As an example, the Michel spectrum obtained with the beam intensity reduced and sweeping magnet off is shown in Fig. 6. The fit with a Michel spectrum folded with a Gaussian gives a 7.0% (FWHM) resolution. As a check, the NaI spectrum from the normal data was fit with a combination of sources including internal and external bremsstrahlung, positron annihilation in flight and a constant background from accelerator neutrons and cosmic rays. The results are shown in Fig. 7, where the fit region is above 45 MeV and the deviation at lower energies is most likely due to thick target bremsstrahlung from the sweeping magnet's pole faces. In the fit region, the χ^2/F is 1.1, the resolution is consistent with the calibrations (7.2% FWHM), and the normalization is consistent with the stop rate to 10%.

The angular correlation measurement depends on both the positron and photon arms. Although it is expected that the MWPC's will give accurate reconstruction of the positrons, multiple scattering will introduce a non-negligible uncertainty. The resolution of the MWPC's was measured by looking at decays of muons which were stopped in horizontal and vertical line targets (1 cm wide). The reconstructed targets are shown in Fig. 8, and these spectra lead to a resolution of better than 1 cm. Since the line targets were surveyed, the locations are a check on the absolute position of the chambers.

The algorithm for the entrance point of the γ-rays into the NaI crystals depends very heavily on a Monte Carlo simulation of the electromagnetic shower which leads to the pulses. The algorithm used was a weighting of the crystal coordinates by the observed energy

Table 3. NaI calibration points.

Source	Energy	Fitted Energy	Resolution (%)	Frequency of Measurement
$Pu \rightarrow \alpha + Be \rightarrow {}^{12}C + \gamma$	4.43	4.33	10.0	1/day
$p + {}^{19}F \rightarrow {}^{20}Ne \rightarrow {}^{16}O + \alpha + \gamma$	6.13	5.90	8.0	1/week
$p + {}^{7}Li \rightarrow {}^{8}Be + \gamma$	17.64	17.26	6.7	1/week
$\mu^{+} \rightarrow e^{+} \nu \bar{\nu}$ (endpoint)	52.83	52.83	7.0	1/day
$\pi^{-} + p \rightarrow \pi^{o} + n$	55.10	55.05	7.5	twice
$\hookrightarrow \gamma\gamma$ (collinear)	82.65	82.43	6.5	twice
$\pi^{-} + p \rightarrow n + \gamma$	129.36	128.30	5.5	twice

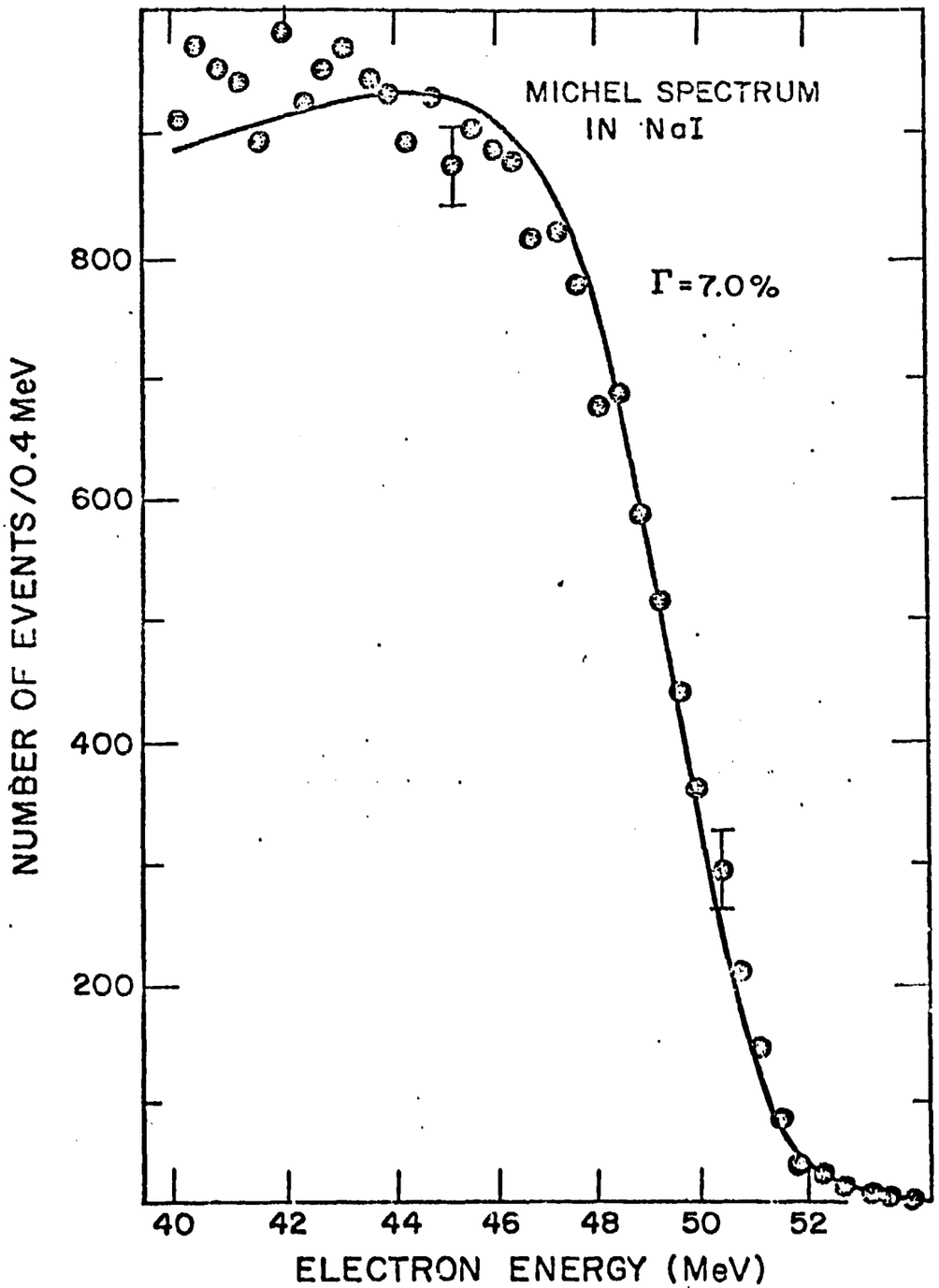

Fig. 6. Michel spectrum in the NaI with the sweeping magnet off.

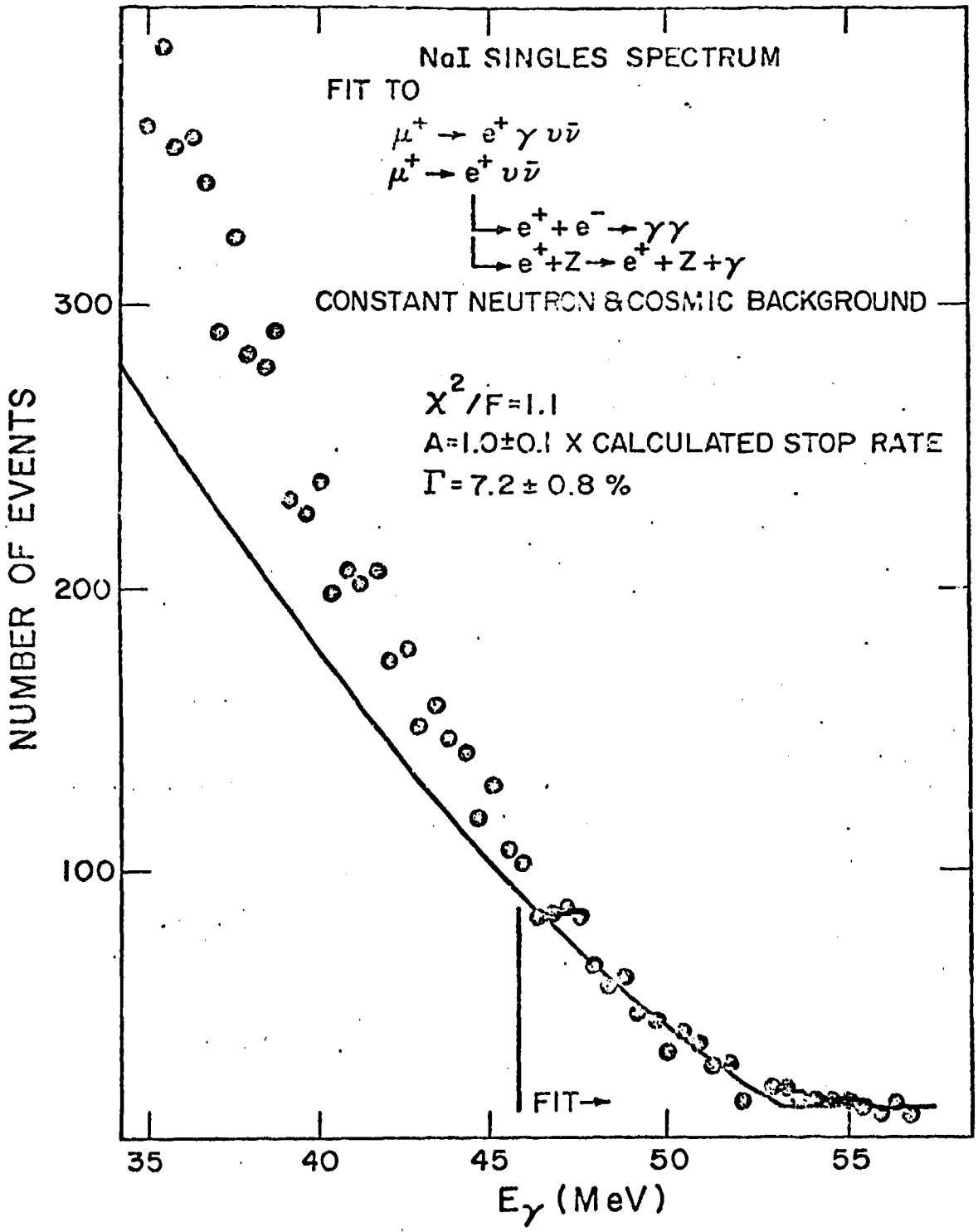

Figure 7. NaI singles spectrum and a fit from known sources of photons.

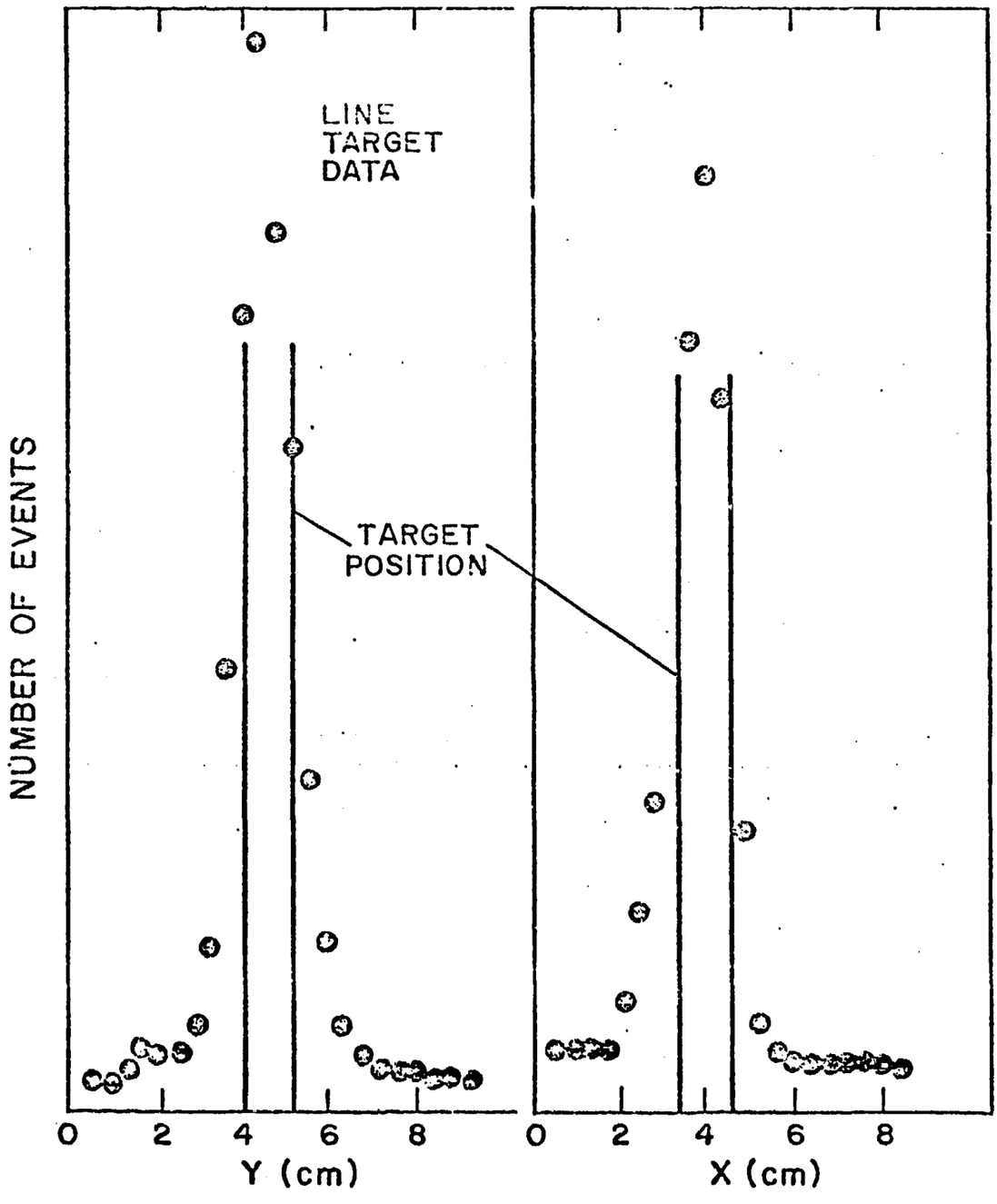

Figure 8. Reconstructions of 1 cm wide horizontal and vertical line targets as determined from detecting the positrons from muon decay.

deposition

$$\vec{x} = \sum_{i=1}^{7} \vec{x}_i E_i^S \Big/ \sum_{i=1}^{7} E_i^S \quad , \tag{2}$$

where S is determined by the matching of mean lateral shower spread to the size of the NaI modules. Monte Carlo calculations suggest $s \simeq 0.4$ and that the mean interaction depth is 4 radiation lengths into the crystals.

In order to fine tune the algorithm empirically for 55 MeV γ-rays, the face of the NaI was covered with a 5 cm thick wall of Pb. In the wall a 2.5 cm high slot of CH_2 was left for coincident photons from π^o decay to pass. The setup is illustrated in Fig 5. For a substantial fraction of the events, no shower leakage into neighboring crystals occurs. The best estimator for these events is a crystal center, and this produces a peak in the projected position spectrum. The spectrum, when projected to the right, is given in Fig. 9. The best Monte Carlo prediction for the data ($s \simeq 0.36$) is also shown. The Monte Carlo is then used to calculate the positron resolution, and the projected resolution is 7 cm FWHM.

With the resolutions and calibrations in hand, the data analysis may proceed. The operating conditions of the experiment are listed in Table 4, and the results reported here represent an analysis of about half the data. A first editing of that part of the data has yielded 8518 events for use with the most refined algorithms and likelihood analysis.

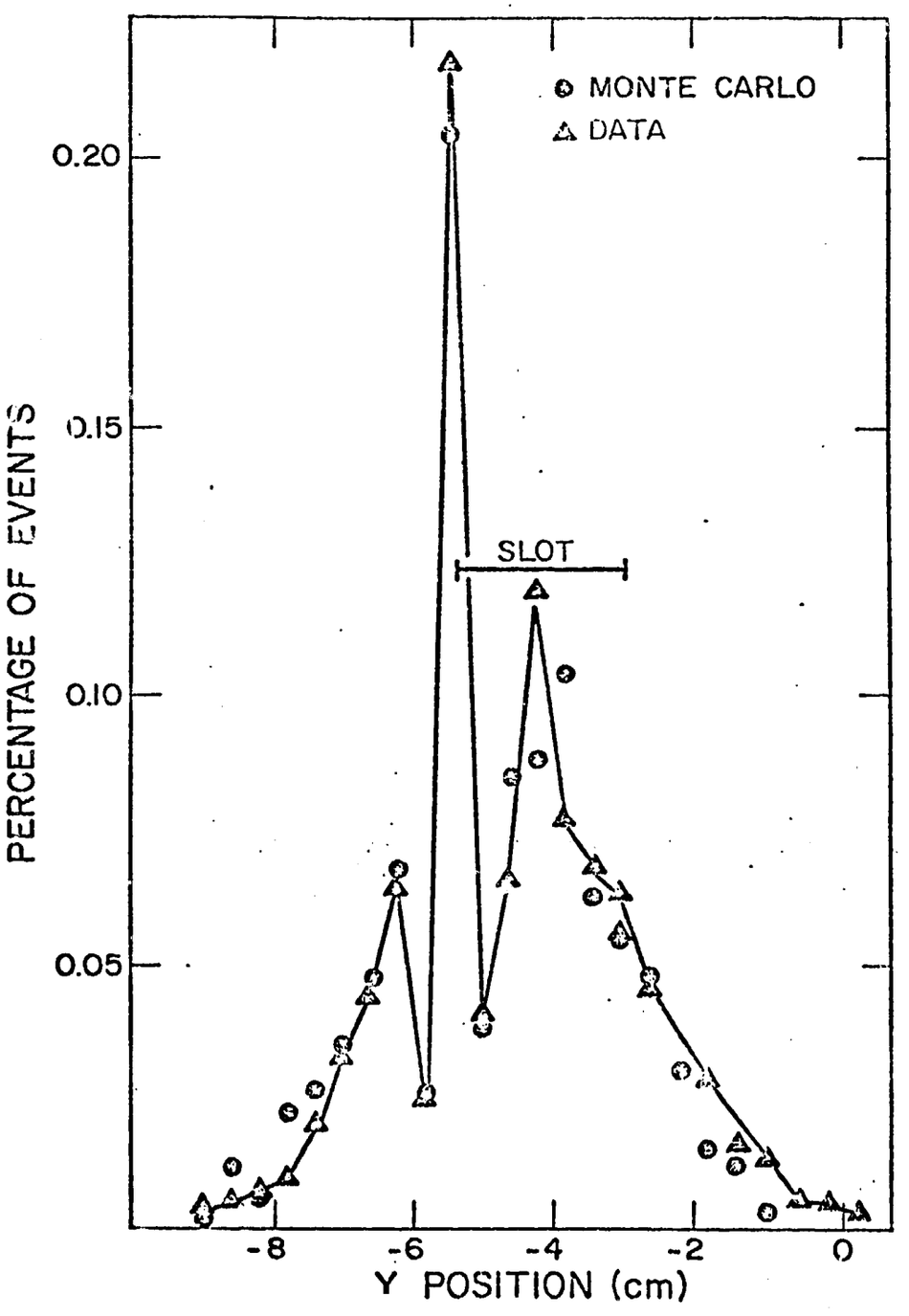

Figure 9. Position data and Monte Carlo simulations for the CH_2 slot in the Pb wall.

Table 4. Typical operating characteristics of the apparatus.

Rates	
Instantaneous μ^+ stops	3.3×10^7/sec
Average μ^+ stops	2.0×10^6/sec
Electron contamination	10%
Instantaneous e^+ triggers	1.4×10^6/sec
Instantaneous γ triggers/NaI crystal	10^3/sec
Triggers	10/sec
Solid Angle	2%
Efficiency for reconstruction	x 60%
	1.2%
μ^+ stops in sample reported	2.3×10^{12}
μ^+ examined in sample reported	3×10^{10}
Events on tape	6×10^6
400 Tapes production data	
250 Tapes calibration data	
Hardware Cuts	$E_\gamma > 35$ MeV
	-10 nsec < t < 10 nsec

If one were to make sharp cuts on all the kinematic variables at 1.5 σ, then one finds 8 events fall in the window. A background of 9 events are expected and this yields a net for $\mu^+ \to e^+\gamma$ of $-1 \pm \sqrt{8}$ events. The branching ratio upper limit at 90% confidence is then given as 1.5 times the number of $\mu^+ \to e^+\gamma$ events divided by the cut efficiency and the number of μ decays examined. This would yield $\Gamma(\mu^+ \to e^+\gamma)/\Gamma(\mu^+ \to \text{all}) \leq 2.9 \times 10^{-10}$.

The proper way to set the limit is to do a maximum likelihood analysis. The experiment is sensitive to three processes: $\mu^+ \to e^+\gamma$, $\mu^+ \to e^+\gamma\nu\bar{\nu}$, and random coincidences. Hence, the likelihood function may be written

$$L(\alpha,\beta) = \frac{1}{N^N} \prod_{i=1}^{N} [\alpha P(x_i) + \beta Q(x_i) + (N-\alpha-\beta) R(x_i)], \tag{3}$$

where N is the total number of events (8518), α is the number of $\mu^+ \to e^+\gamma$ events, β is the number of internal bremsstrahlung events, and x_i are the measured properties of the i^{th} event (E_e, E_γ, $\theta_{e\gamma}$, t). P(x), Q(x), and R(x) are probability density functions for $\mu \to e\gamma$, internal bremsstrahlung, and random events, respectively. P(x) is taken as a product of the measured resolution functions; Q(x) is taken from Q.E.D. calculations of internal bremsstrahlung smeared with the measured resolution functions; R(x) is taken as the product of the shapes of the spectra of the individual parameters. $L(\alpha,\beta)$ can than be interpreted at the joint probability density for α and β.

Figure 10 shows the likelihood contours for α and β. The amount of internal bremsstrahlung observed is consistent with the geometry

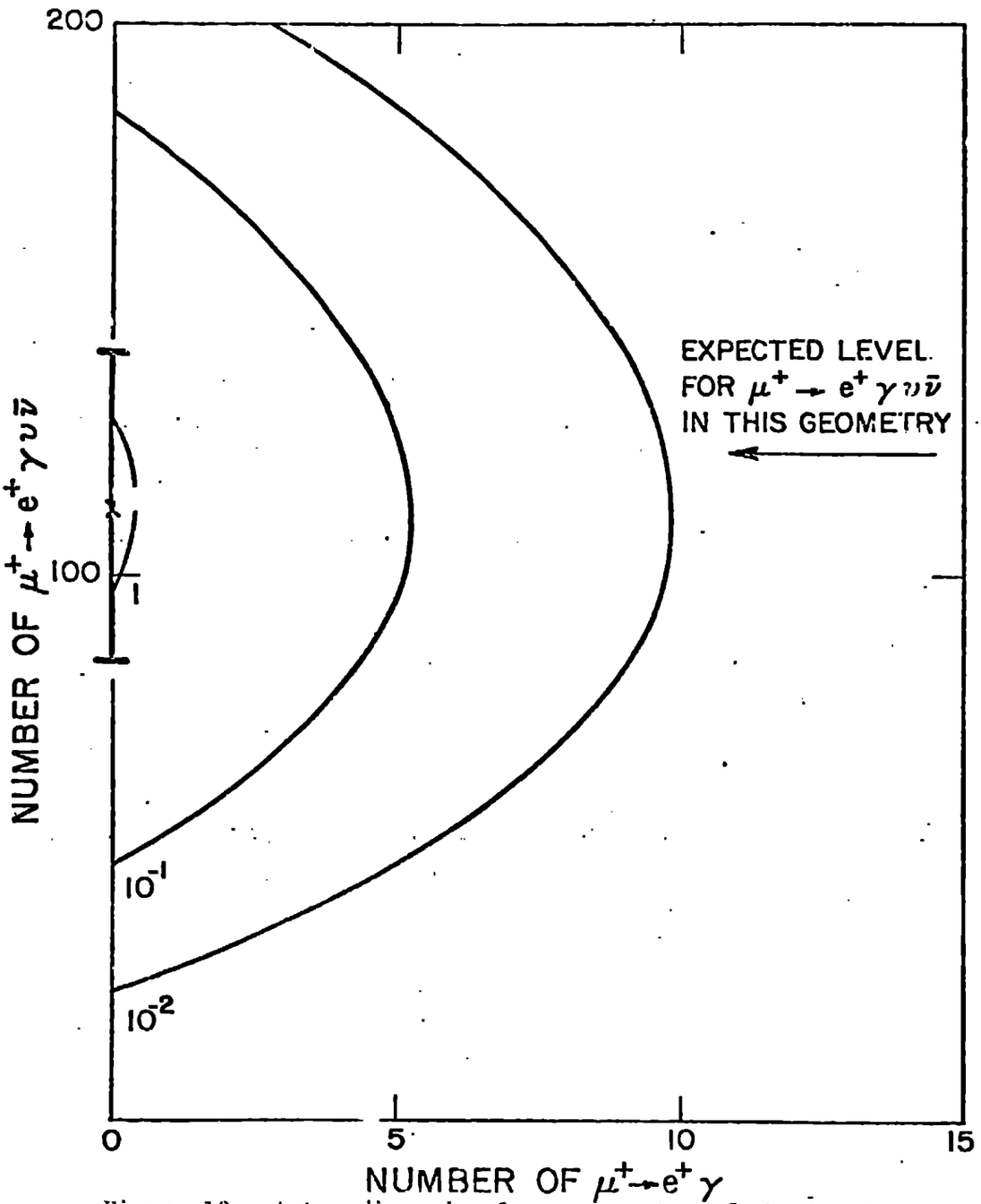

Figure 10. A two dimensional contour plot of the likelihood function's dependence on α, the number of $\mu^+ \to e^+ \gamma$, and β, the number of $\mu^+ \to e^+ \gamma \nu \nu$.

for observing that decay. The fact that the contours are symmetric about horizontal and vertical axis shows that α and β are linearly independent; i.e., the signature for internal bremsstrahlung is distinct from that for $\mu^+ \to e^+\gamma$.

Figure 11 shows the projection of Fig. 10 which displays the dependence on α, and is labeled t=0. The curve labeled t=5 nsec is a likelihood function for purely random events and is consistent with the t=0 curve in accordance with the statistics of small numbers. The 90% confidence limit is the point where the area under the curve is 90% of the total area. This occurs at α=6 events. Hence, after dividing by the number of examined decays, the upper limit for $\mu^+ \to e^+\gamma$ is $\Gamma(\mu^+ \to e^+\gamma)/\Gamma(\mu^+ \to \text{all}) \leq 2.0 \times 10^{-10}$ with 90% confidence.

The physicists who have performed this experiment would like to acknowledge the encouragement and support of Dr. Louis Rosen and the LAMPF administration as well as the many people who provided invaluable technical support throughout the experiment. This project was carried out under the auspices of the U.S. Department of Energy, the National Science Foundation (Grants #PHY77-20610 and #PHY76-10287) and the U.S. National Aeronautics and Space Administration (Grant NGR452).

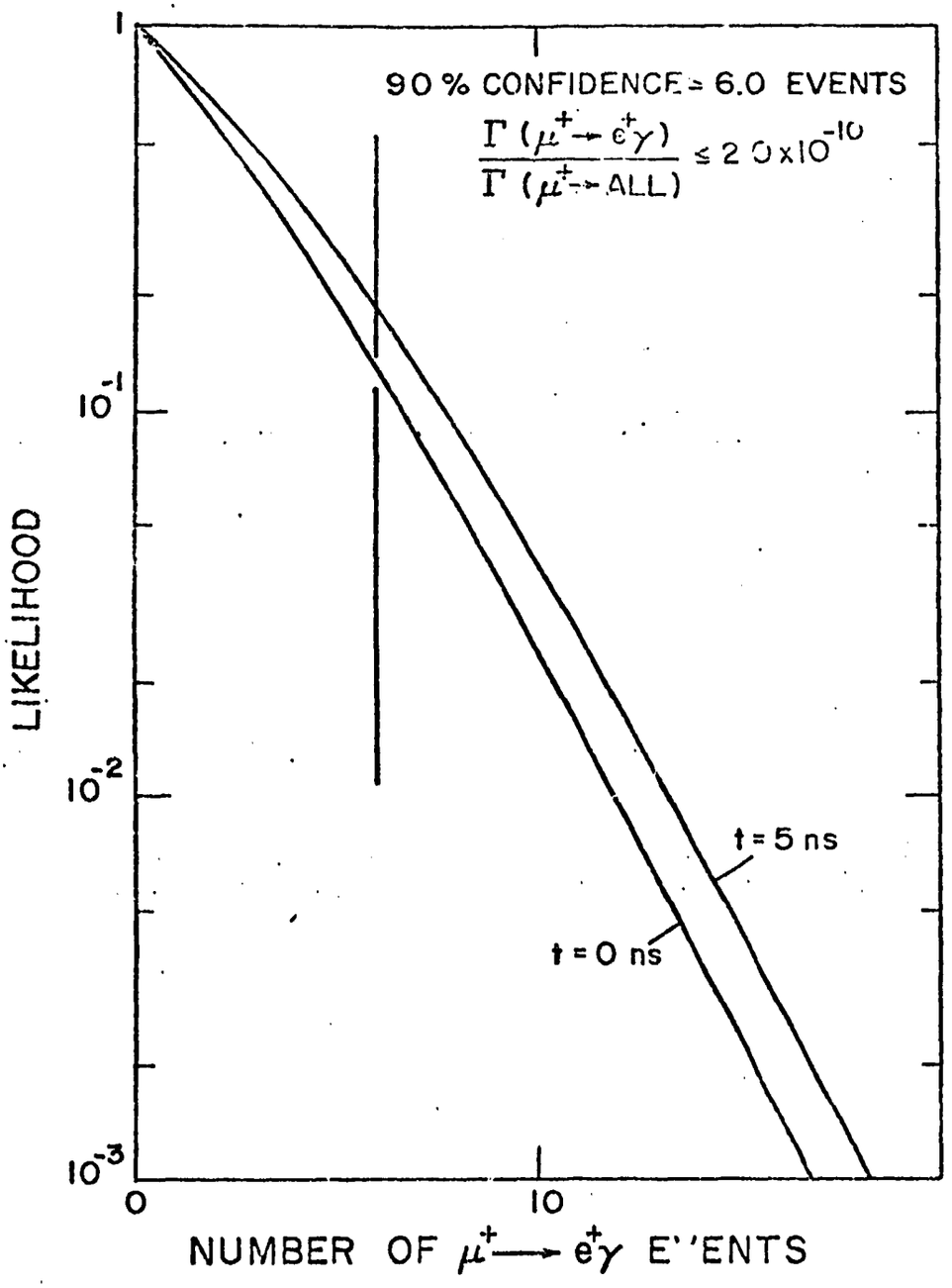

Figure 11. The likelihood function's dependence on α, the number of $\mu^+ \to e^+\gamma$ for coincidence and random events. The vertical line indicates the point where 90% of the likelihood occurs; i.e., at 6 events.

REFERENCES

1. P. Depommier, J. P. Martin, J. M. Poutissou, R. Poutissou, D. Berghofer, M. D. Hasinoff, D. F. Measday, M. Solomon, D. Bryman, M. Dixit, J. A. McDonald, and G. I. Opat, Phys. Rev. Lett. 39, 1113 (1977).

2. J. P. Pevel, W. Dey, H. K. Walter, H. J. Pfeiffer, V. Sennhauser, J. Egger, H. J. Gerber, M. Salzmann, A. Van der Schaat, W. Eichenberger, R. Engfer, F. Hermes, F. Schleputz, V. Weidmann, C. Petitjean and W. Hesselink, Phys. Lett. 72B, 183 (1977).

3. A. Badertscher, K. Borer, G. Czapek, A. Flückiger, H. Hänni, B. Hahn, E. Hugentobler, A. Markees, U. Moser, R. P. Redwine, J. Schacher, H. Scheidiger, P. Schlatter, and G. Viertel, Phys. Rev. Lett. 39, 1385 (1977).

4. M. L. Perl, G. S. Abrams, A. M. Boyarski, M. Breidenbach, D. D. Briggs, F. Bulos, W. Chinowsky, J. T. Dakin, G. J. Feldman, C. E. Friedberg, D. Fryberger, G. Goldhaber, G. Hanson, F. B. Heile, B. Jean-Marie, J. A. Kadyk, R. R. Larsen, A. M. Litke, D. Lüke B. A. Lulu, V. Lüth, D. Lyon, C. C. Morehouse, J. M. Paterson, F. M. Pierre, T. P. Pun, P. A. Rapidis, B. Richter, B. Sadoulet, R. F. Schwitters, W. Tanenbaum, G. H. Trilling, F. Vannucci, J. S. Whitaker, F. C. Winkelmann, and J. E. Wiss, Phys. Rev. Lett. 35, 1489 (1975).

5. T. P. Cheng and L. F. Li, Phys. Rev. D16, 1425 (1977).

6. J. D. Bjorken and S. Weinberg, Phys. Rev. Lett. 38, 622 (1977).

7. J. D. Bowman, T. P. Cheng, L. F. Li, and H. S. Matis, Phys. Rev. Lett. 41, 442 (1978).

8. S. M. Korenchenko, B. F. Kostin, G. V. Mitsel'makher, K. G. Nekrasov, and V. S. Smirnov, JETP 43, 1 (1976).